Synthetic gauge fields in synthetic dimensions

A. Celi,[1] P. Massignan,[1] J. Ruseckas,[2] N. Goldman,[3] I. B. Spielman,[4,5] G. Juzeliūnas,[2] and M. Lewenstein[1,6]

[1] *ICFO – Institut de Ciències Fotòniques, Mediterranean Technology Park, E-08860 Castelldefels (Barcelona), Spain*
[2] *Institute of Theoretical Physics and Astronomy, Vilnius University, A. Goštauto 12, Vilnius 01108, Lithuania*
[3] *Center for Nonlinear Phenomena and Complex Systems - Université Libre de Bruxelles, 231, Campus Plaine, B-1050 Brussels, Belgium*
[4] *Joint Quantum Institute, University of Maryland, College Park, Maryland 20742-4111, USA*
[5] *National Institute of Standards and Technology, Gaithersburg, Maryland 20899, USA*
[6] *ICREA – Institució Catalana de Recerca i Estudis Avançats, E-08010 Barcelona, Spain*

(Dated: November 19, 2013)

SUPPLEMENTAL MATERIAL

Edge states in thin stripes: Hofstadter square lattice vs Hofstadter ladder

In the main text, we have concentrated on the spectra and edge-state dynamics for spin 1 atoms ($F = 1$). In that case a synthetic 2D lattice is constituted of $N \times 3$ lattice sites, where $3 = W = 2F + 1$ is the number of sites along the synthetic (spin) direction and N is the number of sites along the spatial direction x (see Figs. 1 – 3 in the main text). Such a lattice has natural open boundaries along the spin direction at $y = \pm Fa$ (where a is the lattice spacing), while N can be arbitrarily large. In this Appendix, we illustrate how the edge-state properties discussed in the main text can be related to the topological band structure and chiral edge states of the standard Hofstadter square lattice [1], namely, a square lattice of $N \times W$ sites, with $N, W \gg 1$, subjected to a uniform magnetic flux Φ per plaquette. The number of lattice sites along the y direction is denoted W, so as to refer to the width of the stripe.

To do so, we consider an extrapolation between the Hofstadter lattice (size $N \times W$) and the thin stripe considered in the main text (size $N \times 3$), by progressively reducing the number of lattice sites along the y direction W, while applying periodic boundary conditions along the x direction, see Fig. 1 (a). The first spectrum shown in Fig. 1 (b), obtained for $W = 50$, shows the usual band structure of the Hofstadter model, where a clear distinction between the bulk bands and the edge states dispersions is observed. To highlight this edge/bulk picture, we simultaneously represent the energies $E = E(q)$ together with the mean position $\langle y \rangle$ of the eigenstates along the spin direction, see the color code in Fig. 1 (a). The many bulk states progressively disappear, as the number of inequivalent lattice sites is reduced to $W = 5$, while the dispersion branches of the edge states are only slightly modified. In fact, for $\Phi = p/q \in \mathbb{Q}$, the edge-state branches remain remarkably robust for $W \to q$. When W is further reduced such that $W < q$, the edge-state branches are altered, but they retain their general characteristics: in the thin stripe ("double-ladder") limit $W = 3$ considered in the main text, the lowest energy band describes edges states localized on opposite edges (at $y = \pm a$) of the double-ladder, propagating in opposite directions. Therefore, we can conclude that the edge-state structure present in the double-ladder lattice ($W = 3$) is reminiscent of the chiral (topological) edge states present in the standard Hofstadter square lattice (see also Ref. 2 for a detailed study of the Hofstadter ladder with $W = 2$ corresponding to $F = 1/2$).

Experimental realization

Inhomogeneity in the synthetic dimension

In deriving the atomic Hamiltonian Eq. (3) in the main text, we have assumed that the synthetic dimension is homogeneous, i.e. that all spin-dependent energy shifts can be neglected. In a real experiment, (i) quadratic Zeeman shift and also (ii) detuning errors can induce such shifts of the atomic hyperfine states. These terms are equivalent to an effective trapping (or anti trapping) potential along the synthetic dimension. It is consistent to neglect this potential when it is small or comparable to the band width. A typical hopping strength is $\sim 0.1E_L$, giving a $0.4E_L$ band width along one direction. For typical atomic parameters this can be of order ~ 1 kHz. Regarding (i), for instance in ^{87}Rb's F=1 manifold, the quadratic shift (which will be "trapping" in the synthetic direction) can be safely neglected for fields below about $3G$. Regarding (ii), the absolute field stability generally gives detuning uncertainties and noise at the 100 Hz level (and less under exceptional conditions where great care is taken to stabilize the field, see Ref. [3]). As a result, we conclude that both effective trapping contributions of (i) and (ii) should not significantly affect the proposed scheme.

Temperature requirements

In the simulations presented in this paper, we have restricted ourselves to the zero temperature case. We ad-

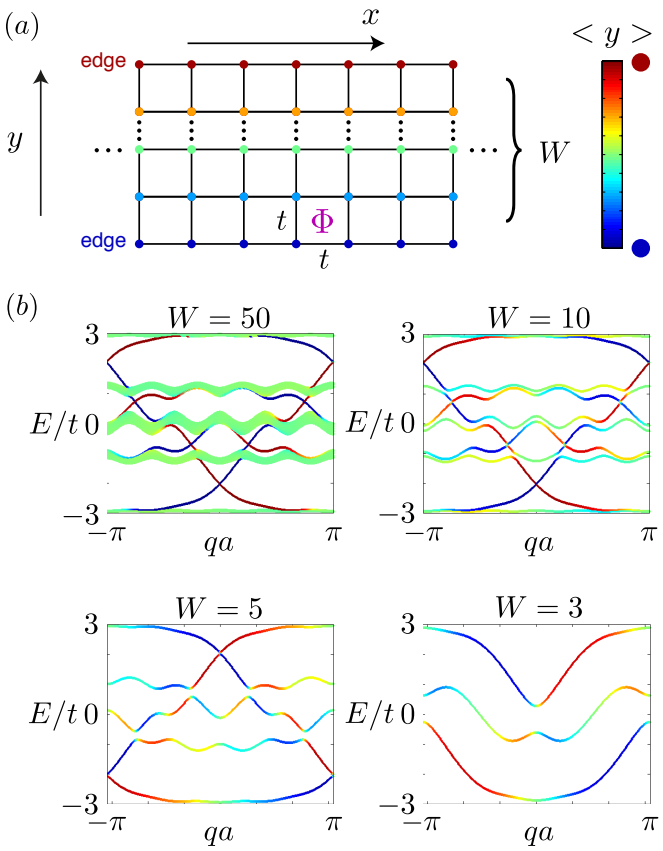

FIG. 1. (a) Hofstadter model on a stripe of width W, and definition of the color code: dark blue (resp. red) dots correspond to states localized at the bottom (resp. top) edge of the system, whereas green-yellow dots correspond to bulk states. (b) Energy spectrum $E = E(q)$ of the Hofstadter model with the flux $\Phi = 1/5$, for different stripe widths W. Here, the modulus of the hopping amplitude is taken equal to t along both directions, and q denotes the quasi-momentum. The double-ladder configuration used in the main text corresponds to $W = 3$ (i.e., $F = 1$ and $\Omega_0 = t$).

dress here the validity of this approximation, when comparing to realistic experimental conditions.

The detection of a clear edge-state signal, namely, observing the propagation of particles characterized by a unique chirality along the "edges", requires that the temperature should be smaller than the energy separation between states localized on the same edge (or spin state $\pm F$, as shown by red and blue colors in Fig. 2 of the main text, and Figs. 1-2 of the present Supplemental Material) and propagating in opposite directions. For the parameters in Fig.2(b) of the main text, $\Omega = 0.5t$, such excitations lie approximately $2t$ above the Fermi energy (the dashed horizontal line). Moreover, to improve the signal it is also important not to populate dispersive "bulk" states, thus temperatures should also be small compared to the energy separation between the low-energy (almost dispersionless) bulk states and higher-energy dispersive states. This separation is of order t, i.e., this condition imposes the most stringent requirement. For typical experimental realizations, the tunneling t is of order $\sim$ 10nK. As such, the temperature of the system should be at most of order of a few nK.

The $F = 9/2$ case

In the main text, we focused on the study of the $F = 1$ case, which is widely investigated in current cold-atom experiments [4, 5]. This leads to the double-ladder lattice, whose connection with the standard Hofstadter model has been described in the previous Section of this Supplementary material. However, it would be desirable to engineer a synthetic 2D lattice with more internal states to make this connection even more visible. For example, considering the ground-state manifold of ^{40}K, where $F = 9/2$, would allow to engineer a lattice of size $N \times 10$, which according to Fig. 1 (b) would clearly display the topological band structure of the Hofstadter model. We note that using other atomic species (such as ^{173}Yb) could also lead to similar configurations with $W > 5$, both for bosonic and fermionic systems.
One important aspect of the present proposal is the fact that for $F > 1$ the magnitude of hopping along the y (spin) direction is not constant. Indeed, the hopping from a lattice site m to a lattice site $m + 1$ is given by the frequency

$$t_{m\to m+1} = \Omega g_{F,m} = \Omega\sqrt{F(F+1) - m(m+1)}, \quad (1)$$

where we remind that $m = m$ refers to the internal states of the atom and F is the total angular momentum. This inhomogenous hopping, shown in Fig. 2 (a) for $F = 9/2$, is not present in the standard Hofstadter model, where the tight-binding hopping amplitude t is constant. To illustrate this effect, we show the band structure of a synthetic lattice engineered with $F = 9/2$ atoms (Fig. 2 (b)), and we compare it with the band structure of the homogenous Hofstadter model with $W = 10$ (Fig. 2 (c)). We observe that the bulk/edge band structure is well conserved, when choosing $\Omega = t/\langle g_{F,m}\rangle$, where $\langle g_{F,m}\rangle = \sum_m g_{F,m}/2F$. However, we note that the states corresponding to the edge-state dispersions are no longer perfectly localized at the edges: close to the lowest bulk band, there are dispersive states with $|\langle m\rangle| < 9/2$. We also note that the states with the highest velocity $v \sim \partial_q E$ are those that are the most localized at the edges.

In Fig. 3, we show the edge-state dynamics for a fermionic system with $F = 9/2$ atoms (e.g. ^{40}K), confined by a harmonic potential $V_{\rm harm}(x) = t(x/50a)^2$. We clearly observe a chiral motion in the 2D synthetic lattice, which is due to the populated edge states lying within the lowest bulk gap (Fig. 2 (b)). As already described above, these edge states are not perfectly localized at $m = \pm 9/2$, due to the inhomogeneity of the hopping along the spin

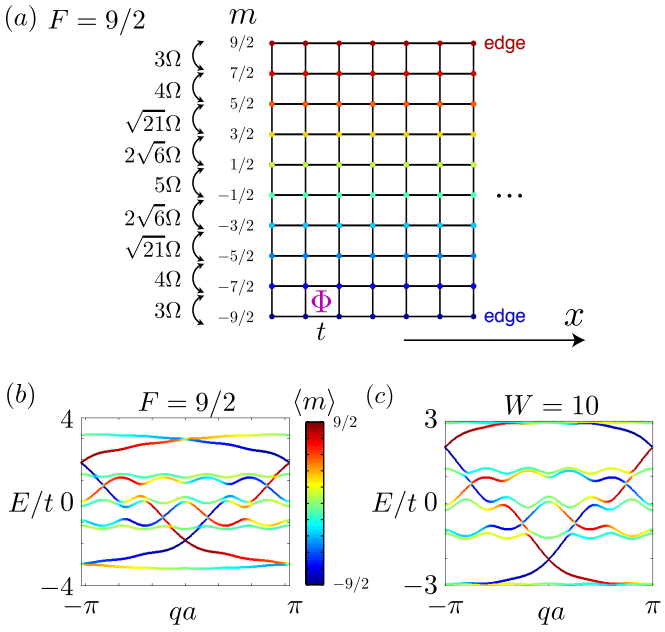

FIG. 2. (a) Synthetic lattice for $F = 9/2$ atoms. The hopping amplitude t along the x (spatial) direction is constant, while the hopping amplitude along the y (spin) direction, $\Omega g_{F,m}$, is given by Eq. (1). (b) The energy spectrum for the $F = 9/2$ synthetic lattice, setting $\Phi = 1/5$ and $\Omega = t/\langle g_{F,m}\rangle = 0.24t$. (c) The energy spectrum for the homogenous Hofstadter lattice with $W = 10$ lattice sites along the y direction and $\Phi = 1/5$, see also Fig. 1b. Note that the edge states are more spatially localized in the homogeneous case [(c)] than in the inhomogeneous synthetic lattice [(b)].

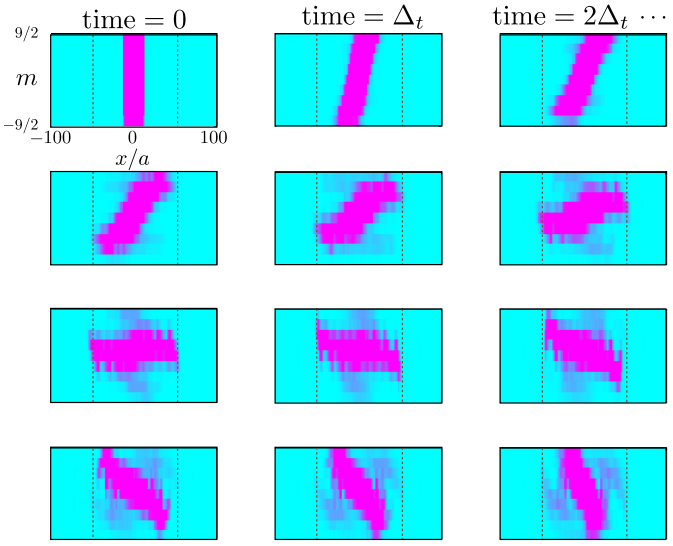

FIG. 3. Edge-states dynamics for a fermionic system with $F = 9/2$ atoms (e.g. ^{40}K): the Fermi gas is trapped in the central region $x \in [-13a, 13a]$ and the Fermi energy is set such as to populate only the lowest energy band. The populated "edge" states localized at $m = \pm F$ have opposite group velocities. An additional harmonic potential limits the edge-states propagation, leading to chiral dynamics around the synthetic 2D lattice. The parameters are $\Omega = t/\langle g_{F,m}\rangle = 0.24t$, $\Phi = 1/5$, $V_{\rm harm}(x) = t(x/50a)^2$ and $E_{\rm F} = -2t$. Dashed lines represent the Fermi radius $R_{\rm F}$ at which the edge states localized at $m = \pm F$ jump unto the opposite edge $m = \mp F$. The time steps are $\Delta_t = 37.5\hbar/J$.

direction. As a result, the dynamics show the rotation of the cloud in the 2D lattice, instead of a clear edge-state motion.

Scattering on a localized impurity

Formulation

Our aim here is to calculate the transmission probability for an atom in the 1D physical lattice affected by an impurity localized at $n = 0$ and thus described by the Hamiltonian

$$H_{\rm imp} = H + V\,, \quad V = \sum_{m,m'} V_{m,m'} a^\dagger_{0,m} a_{0,m'}\,, \qquad (2)$$

where H is an unperturbed Hamiltonian for the 1D array of atoms is given by Eq.(3) of the main text, and m refers to the spin levels representing a synthetic degree of freedom.

We shall make use of the Green's operator $G = [E - H_{\rm imp} + i0^+]^{-1}$ of the full Hamiltonian $H_{\rm imp}$. The Green's operator of the complete system will be expressed in terms of the Green's operator $G_0 = [E - H + i0^+]^{-1}$ of the unperturbed system using the Dyson equation [6] $G = G_0 + G_0 V G$. On the other hand, the zero-order Green's operator G_0 will be presented via the eigenfunctions and eigen-energies of the unperturbed Hamiltonian H. Having the complete Green's operator G we will determine the scattering T-matrix $T = V + VGV$ from which the transmission probabilities will be calculated.

Spectrum of the Hamiltonian without impurity

Applying a gauge transformation $\tilde{a}_{n,m} = a_{n,m} e^{-i\gamma nm}$ we transfer the phases featured in the hopping elements to the hopping in the physical direction in the Hamiltonian H defined by Eq. (3) in the main text, giving:

$$H = \sum_{n,m} \left(-te^{-i\gamma m} \tilde{a}^\dagger_{n+1,m} + \Omega_{m-1} \tilde{a}^\dagger_{n,m-1} \right) \tilde{a}_{n,m} + \text{H.c.}\,. \qquad (3)$$

From now on we will express all energies in the units of the hopping integral t; therefore, we will set $t = 1$. The atomic center-of mass wave function satisfies the Schrödinger equation

$$H\Psi = E\Psi\,. \qquad (4)$$

We search for the eigenvectors of the Hamiltonian (3) in the form of plane waves (Bloch states) by taking the probability amplitudes to find an atom in the site n, m as

$$\Psi_m(n) = \chi_{q,m} e^{iqn} \,. \tag{5}$$

We will interpret the index m as a row number and consider Ψ and χ_q as columns. Equation (4) yields the following eigenvalue equations

$$H_q \chi_q = E_q \chi_q \,.$$

Here H_q is $(2F+1) \times (2F+1)$ matrix with the diagonal matrix elements $(H_q)_{m,m} = -2\cos(q + \gamma m)$ and nonzero non-diagonal elements $(H_q)_{m,m'} = \Omega_m \delta_{m',m+1}$ and $(H_q)_{m,m'} = \Omega_{m-1}\delta_{m',m-1}$. In particular, when $F = 1$ the matrix H_q reduces to

$$H_q = \begin{pmatrix} -2\cos(q-\gamma) & \Omega & 0 \\ \Omega & -2\cos(q) & \Omega \\ 0 & \Omega & -2\cos(q+\gamma) \end{pmatrix} . \tag{6}$$

By solving an eigenvalue problem we get a set of $2F+1$ algebraic equations. It has has $2F+1$ solutions to be labelled with an index ν.

Green's function of the system without impurity

Given the eigenfunctions $\Psi_{q,s}(n)$, the general expression for the retarded zero-order Green's function is

$$G_0(n, n'; E) = \sum_{\nu=1}^{2F+1} \int_{-\pi}^{\pi} \frac{\Psi_{q,\nu}(n)\Psi^*_{q,\nu}(n')}{E - E_{q,\nu} + i\eta} dq \,, \tag{7}$$

where $\eta \to +0$. Zeros in the denominator can be obtained from the eigen-energy equation

$$\det[E - H_q] = 0 \,, \tag{8}$$

which generally has $2F+1$ solutions. For each eigenenergy E and wave vector q_ν, the analytical expressions for the eigenvectors $\chi_{q_\nu,\nu}$ can be obtained from the equation $[H_q - E]\chi_{q_\nu,\nu} = 0$ by setting the first element of $\chi_{q_\nu,\nu}$ to unity and dropping one of the resulting equations. Using Eq. (7) and performing the integration we obtain the retarded zero-order Green's function

$$G_0(n, n'; E) = -i \sum_\nu \frac{1}{v_\nu} \begin{cases} \chi_{q_\nu,\nu}\chi^T_{q_\nu,\nu} e^{iq_\nu(n-n')} \,, & n > n', \\ \chi_{-q_\nu,\nu}\chi^T_{-q_\nu,\nu} e^{-iq_\nu(n-n')} \,, & n < n', \end{cases} \tag{9}$$

Here

$$v_\nu \equiv \left. \frac{\partial}{\partial q} E_{q,\nu} \right|_{q=q_\nu} \tag{10}$$

is the group velocity. It can be calculated from the equation

$$v_\nu = - \left. \frac{\frac{\partial}{\partial q}\det[E - H_q]}{\frac{\partial}{\partial E}\det[E - H_q]} \right|_{q=q_\nu} . \tag{11}$$

Note that we do not have complex conjugation in Eq. (9) since for real wave vectors q_ν the colums $\chi_{q_\nu,\nu}$ are real. This is because the Hamiltonian H_q has real matrix elements.

Green's function for the system with localized impurity

Combining the Dyson equation $G = G_0 + G_0 V G$ with Eq. (2) for V, one has

$$\begin{aligned} G(n, n') &= G_0(n, n') + \sum_{n''} G_0(n, n'') V \delta_{n'',0} G(n'', n') \\ &= G_0(n, n') + G_0(n, 0) V G(0, n') \,. \end{aligned} \tag{12}$$

Taking $n = 0$ in Eq. (12) we get

$$G(0, n') = G_0(0, n') + G_0(0, 0) V G(0, n') \,. \tag{13}$$

From here we obtain

$$G(0, n') = [1 - G_0(0, 0)V]^{-1} G_0(0, n') \,. \tag{14}$$

Substituting Eq. (14) back into Eq. (12) we get the required expression for the Green's function

$$G(n, n') = G_0(n, n') + G_0(n, 0) V [1 - G_0(0, 0)V]^{-1} G_0(0, n') \,. \tag{15}$$

Transmission probabilities

The scattering is described by T matrix

$$T = V + VGV \,. \tag{16}$$

Using Eq. (15), T matrix reads

$$T(n, n') = V[1 - G^{(0)}(0, 0)V]^{-1} \delta_{n,0} \delta_{n',0} \,. \tag{17}$$

For transmitted waves the matrix element of the scattering matrix is

$$S^t_{\nu,\nu'} = \delta_{\nu,\nu'} - i\frac{1}{\sqrt{v_\nu v_{\nu'}}}\sum_{n,n'}\chi^\dagger_{q_\nu,\nu}e^{-iq_\nu n}T(n,n')\chi_{q_{\nu'},\nu'}e^{iq_{\nu'}n'}\,. \tag{18}$$

Using Eq. (17) we obtain

$$S^t_{\nu,\nu'} = \delta_{\nu,\nu'} - \sqrt{\frac{v_\nu}{v_{\nu'}}}i\frac{1}{v_\nu}\chi^\dagger_{q_\nu,\nu}V\left[1 + i\sum_{\nu''}\frac{1}{v_{\nu''}}\chi_{q_{\nu''},\nu''}\chi^\dagger_{q_{\nu''},\nu''}V\right]^{-1}\chi_{q_{\nu'},\nu'}\,. \tag{19}$$

Transmission probability from the propagating mode ν' to the mode ν is

$$T_{\nu,\nu'} = |S^t_{\nu,\nu'}|^2\,. \tag{20}$$

These equations are used in calculating the transmission probabilities in the main text.

[1] Y. Hatsugai, Phys. Rev. Lett. (1993).
[2] D. Hügel and B. Paredes, arXiv:1306.1190 (2013).
[3] Y. J. Lin *et al.*, Nature Phys. **7**, 531 (2011).
[4] Y. J. Lin *et al.*, Nature **462**, 628 (2009).
[5] Y.-J. Lin *et al.*, Phys. Rev. Lett. **102**, 130401 (2009).
[6] E. N. Economou, *Green's Function in Quantum Physics* (Springer, Berlin, Heidelberg, New York, 2006).